Natural Hazards and Earth System Sciences (2002) 2: 239–245

Natural Hazards and Earth System Sciences

A new method for avalanche hazard mapping using a combination of statistical and deterministic models

M. Barbolini[1] **and C. J. Keylock**[1]

[1]Department of Hydraulic and Environmental Engineering, University of Pavia, Via Ferrata 1, I-27100 Pavia, Italy
[2]School of Geography,University of Leeds, Leeds, LS2 9JT, United Kingdom

Received: 20 September 2001 – Revised: 15 January 2002 – Accepted: 16 January 2002

Abstract. The purpose of the present paper is to propose a new method for avalanche hazard mapping using a combination of statistical and deterministic modelling tools. The methodology is based on frequency-weighted impact pressure, and uses an avalanche dynamics model embedded within a statistical framework. The outlined procedure provides a useful way for avalanche experts to produce hazard maps for the typical case of avalanche sites where historical records are either poorly documented or even completely lacking, as well as to derive confidence limits on the proposed zoning. The methodology is implemented using avalanche information from Iceland and the Swiss mapping criteria, and applied to an Icelandic real world avalanche-mapping problem.

1 Introduction

The usual (and sometimes legally required) avalanche hazard mapping procedure for settlements in the mountainous regions of Europe is based upon the Swiss zoning scheme (Salm et al., 1990). Areas of land are allocated to zones with a different degree of danger (red, blue or yellow in descending order of hazard) based upon return period and impact pressure information. The most important boundary in this system is that between the red (high danger) and blue (moderate danger) zones, due to its implication in terms of land use restrictions (BFF/SLF, 1984). This boundary (in the following indicated as $x_{R/B}$) is placed at the position where the expected avalanche return period (T) is 30 years, unless avalanches with return periods between 30 and 300 years exert impact pressures (I) of greater than 30 kPa at this position. In this case, the boundary between the red and blue zones is moved downslope until the expected value of I, for avalanches where $30 \leq T \leq 300$ years, is less than 30 kPa.

Correspondence to: M. Barbolini
(massimiliano.barbolini@unipv.it)

In practice, this evaluation is usually performed by estimating the T = 30 and T = 300 year snow volume in the starting zone (from meteorological data analysis and release zone morphology), and then using this volume as input to an appropriately calibrated avalanche dynamics model to determine the runout distances $x(T = 30$ years) and $x(T = 300$ years) for these two events. Since the dynamics model gives I as a function of position, $x(T = 30$ years) may be compared to $x(I = 30$ kPa) for the T = 300 years event, and whichever is further downslope locates $x_{R/B}$.

There are a number of uncertainties that are inherent in this type of analysis, but which are not explicitly incorporated into avalanche hazard maps:

- estimating the avalanche release volume for a given return period is subject to error, particularly for sites with a short snowfall record;
- if historical avalanche runout information is sparse, as it usually is, model calibration will be problematic and embody error;
- the simulated runout distance could differ from the true value, even if the release volume estimate is exact, due to the inherent variability of the dynamics of otherwise similar avalanche events (a given volume of snow can give a range of expected runout distances depending on the properties of the released snow and the snow cover along the track; that is, for a given runout distance, there is a distribution of avalanche sizes).

This paper demonstrates how different modelling techniques can be properly combined to estimate the hazard limits for poorly documented avalanche paths, and how Monte-Carlo techniques can be used to evaluate the expected error in the estimation of $x_{R/B}$.

2 Method

The proposed method is based on frequency-weighted impact pressure, and uses an avalanche dynamics model em-

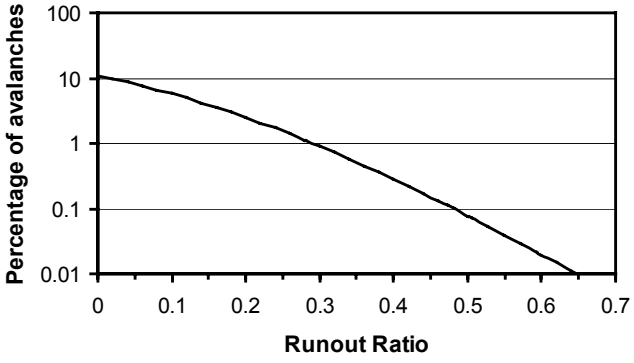

Fig. 1. Avalanches exceedance P (expressed as a percentage) as a function of runout distance (in terms of the runout ratio RR), using the model of Keylock et al. (1999).

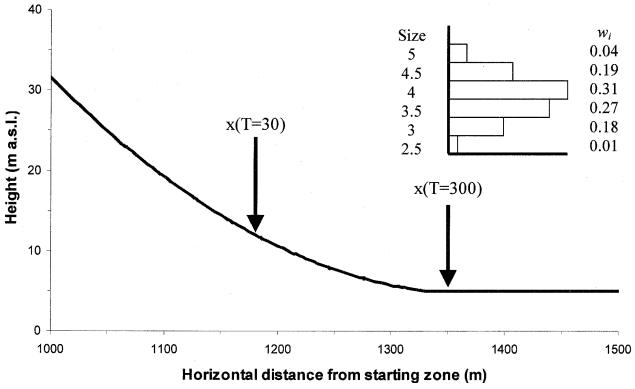

Fig. 2. The relative frequency (wi) of avalanches with different sizes stopping at $x(T = 300$ years) for the Súdavik avalanche path (see Sect. 3); the estimated runout position for the $T = 30$ years avalanche is also indicated. The Canadian classification uses five sizes (1 to 5), although it is common for avalanche observers to use also half sizes; in this work we have followed this approach. In the figure, sizes 1, 1.5 and 2 are not included (i.e. $w_1 = w_{1.5} = w_2 = 0$), because they do not reach $x(T = 300$ years), i.e. in the sense that for these sizes the probability of reaching the target location is below a threshold value (fixed at 0.005).

bedded within a statistical framework. A statistical model for avalanche runout distance (Keylock et al., 1999) is used to obtain avalanche encounter probability as a function of avalanche size and location along the path, as well as to obtain the frequency distribution of avalanche sizes. This model is based on data derived from a number of paths in a mountainous region (Iceland) and gives an "average probability versus runout distance" relation for that region. As such, it is best applied to paths with topographies similar to the majority in the original data set. A hydraulic-continuum avalanche dynamics model (Natale et al., 1994; Barbolini et al., 2000), using a classical two-parameter Voellmy-like resistance law (Bartelt et al., 1999) is tuned to the runout distances provided by the statistical model, and is used to derive impact pressure estimates. Impact pressure is calculated as the product of snow density and velocity squared, according to the proposal of Salm et al. (1990).

The curve of Fig. 1 gives the percentage of avalanche (P) reaching a given position along the path, expressed in terms of the runout ratio, RR (McClung and Lied, 1987). If F indicates the average number of avalanches per year on the considered path, Eq. (1) relates the actual avalanche return periods T and the probability $P/100$ of an avalanche attaining a given runout ratio. Figure 1 gives P as a function of RR, which allows for the runout positions $x(T = 30$ years) and $x(T = 300$ years) to be determined

$$F \cdot \left(\frac{P}{100}\right) = \frac{1}{T}. \tag{1}$$

Within the statistical model of Keylock et al. (1999), different sized avalanches (according to the Canadian size classification, McClung and Schaerer, 1993) can have the same stopping position, but a different probability of stopping at this position (Fig. 2). Therefore, for each avalanche size, the impact pressure at $x(T = 30$ years) is calculated by simulating the dynamics of the different sized avalanches stopping at the location $x(T = 300$ years). If the impact pressure for the size i avalanche is larger than 30 kPa at the $x(T = 30$ years) location, the location xi, where the impact pressure is equal to 30 kPa, is found (Fig. 3), and then the relative frequencies of each size (wi) are used as weights to give the frequency-weighted average position of the red/blue zone boundary, $\overline{x}_{R/B}$ (in the following we will refer to this estimate as Step A of the procedure):

$$\overline{x}_{R/B} = \frac{\sum w_i x_i}{\sum w_i}. \tag{2}$$

Given the distribution of avalanche sizes stopping at $x(T = 300$ years) (Fig. 2), it is also possible to calculate the relative frequencies of the smallest and largest 5% of avalanches (Fig. 4), renormalise this, and use the renormalised probabilities to estimate by Eq. (2) the locations $\overline{x}_{R/B}$ for the smallest and largest 5% of avalanches (given by $\overline{x}_{R/B}(0.05)$ and $\overline{x}_{R/B}(0.95)$, respectively). These latter values can be viewed as approximate 90% bounds on the frequency-weighted average location of the red/blue zone boundary $\overline{x}_{R/B}$ (Step B).

In addition, the uncertainty in the statistical model estimate of $x(T = 30$ years) and $x(T = 300$ years) can be incorporated by concentrating the statistical model error onto the estimate of F. If we assume that the error on F conforms to a symmetric triangular distribution, by Eq. (1) and Fig. 1, the position of $x(T = 30$ years) and $x(T = 300$ years) can be given in terms of (skewed) triangular distributions (Fig. 5). If a value for $x(T = 30$ years) and $x(T = 300$ years) is randomly sampled from their respective distributions and the previously outlined steps are performed, a single estimate for $\overline{x}_{R/B}$, $\overline{x}_{R/B}(0.05)$, and $\overline{x}_{R/B}(0.95)$ is obtained. If we perform the procedure several times by Monte Carlo simulation, it is possible to obtain confidence intervals on the estimate of $\overline{x}_{R/B}$, $\overline{x}_{R/B}(0.05)$ and $\overline{x}_{R/B}(0.95)$ (Step C).

Furthermore, it is possible to obtain the complete Probability Distribution Function (PDF) for $x_{R/B}$ by taking the proba-

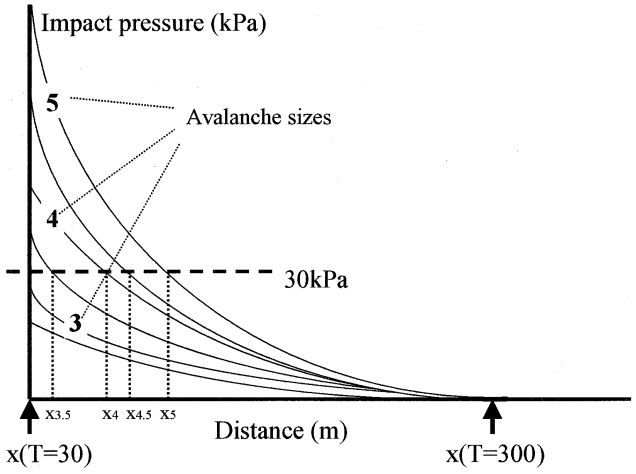

Fig. 3. Impact pressure as a function of distance for different sized avalanches stopping at $x(T = 300$ years). The positions x_i show where the pressure for different sizes (i) reach 30 kPa. If an avalanche size j does not reach 30 kPa by $x(T = 30$ years) (in the figure, this is true for sizes 2.5 and 3), then in Eq. (2), x_j is set to $x(T = 30$ years).

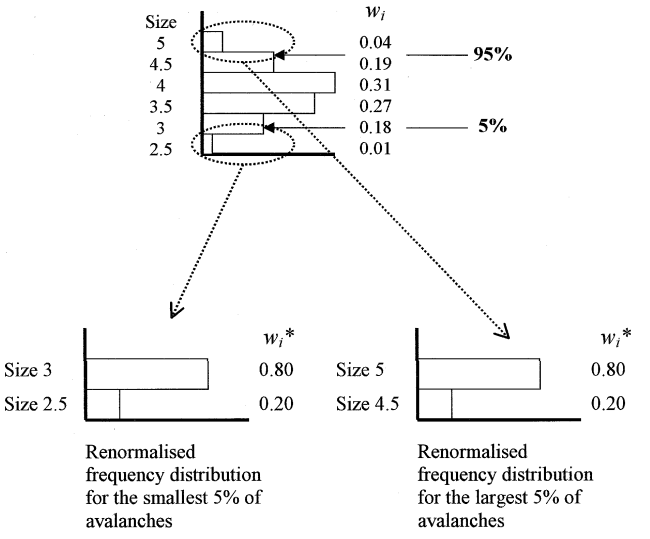

Fig. 4. Derivation of the relative frequency distributions for the upper and lower 5% of avalanches stopping at $x(T = 300$ years), w_i*, from the complete relative frequency distribution, w_i.

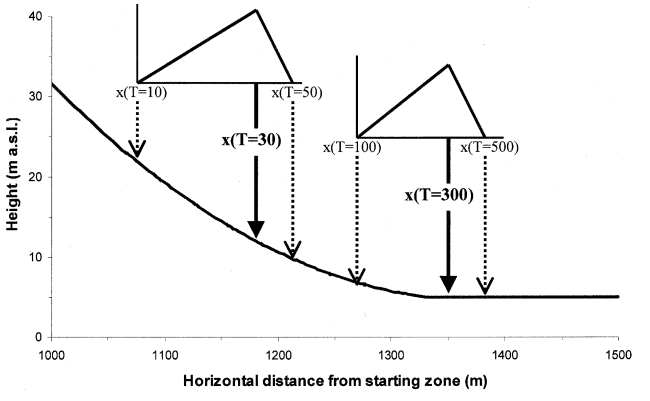

Fig. 5. Triangular distributions for the position of $x(T = 30$ years) and $x(T = 300$ years) due to uncertainty in F. In this study, we assume that the value for F is sufficiently constrained so that the limits for these distributions lie between $x(T = 10$ years) and $x(T = 50$ years) in the former case, and $x(T = 100$ years) and $x(T = 500$ years) for the latter (see Sect. 3).

bility distribution of avalanche sizes at each random estimate for $x(T = 300$ years) (see Fig. 2), selecting one of these sizes at random according to this distribution, and calculating the respective position for $x_{R/B}$ (by comparing $x(I = 30\,\text{kPa})$ for the selected size with the randomly estimated location of $x(T = 30$ years)). Again, if this is repeated many times, the properties of the PDF of $x_{R/B}$ can be inferred (Step D).

3 Application to a study case

On 16 January 1995 an avalanche damaged or destroyed 22 houses from a total of seventy in the village of Súdavik in the northwest of Iceland, killing 14 people. The location of this village in Iceland can be seen in Fig. 1 of Keylock et al. (1999). This avalanche path is used in this paper to illustrate the proposed approach. The calibration procedure for the dynamics model at this site, as well as the combined modelling procedure, is explained in more detail in Keylock and Barbolini (2001).

According to the statistical model, the most probable locations for $x(T = 30$ years) and $x(T = 300$ years) upon this path are 1173 m and 1346 m, respectively, i.e. at elevations above sea level of 12.5 m and 0.0 m, and runout ratios of 0.29 and 0.48. The major limitation of our approach for runout distance estimation is the value for F. Our best-guess value for F was 3.26 (approximately 3) avalanches per year based upon historical avalanche information for this path, with an estimated error of approximately 2 avalanches per year. Hence, the lower and upper limits for the triangular distributions for the error in the estimation of F were given by the locations $x(T = 10$ years), and $x(T = 50$ years) for $x(T = 30$ years) and $x(T = 100$ years) and $x(T = 500$ years) for $x(T = 300$ years), see Fig. 5. These positions equated to values for F of 1.08 and 5.45 avalanches per year for the lower and upper limits, respectively.

Figure 6 shows the results from our procedure calculated in three different ways. The profile shown is that used for the Súdavik path and three results are shown on each plot. Figure 6a shows the values for $\overline{x}_{R/B}$, $\overline{x}_{R/B}(0.05)$ and $\overline{x}_{R/B}(0.95)$ using the best estimates for $x(T = 30$ years) and $x(T = 300$ years) given above (Step A and B of Sect. 2). Figure 6b introduces variability in $x(T = 30$ years) and $x(T = 300$ years) and permits confidence intervals to be placed on the estimates of these three positions (Step C of Sect. 2). Finally, Fig. 6c gives the full PDF for $\overline{x}_{R/B}$ including the 5% and 95% confidence limits (Step D of Sect. 2).

Comparing the results obtained by the two different types

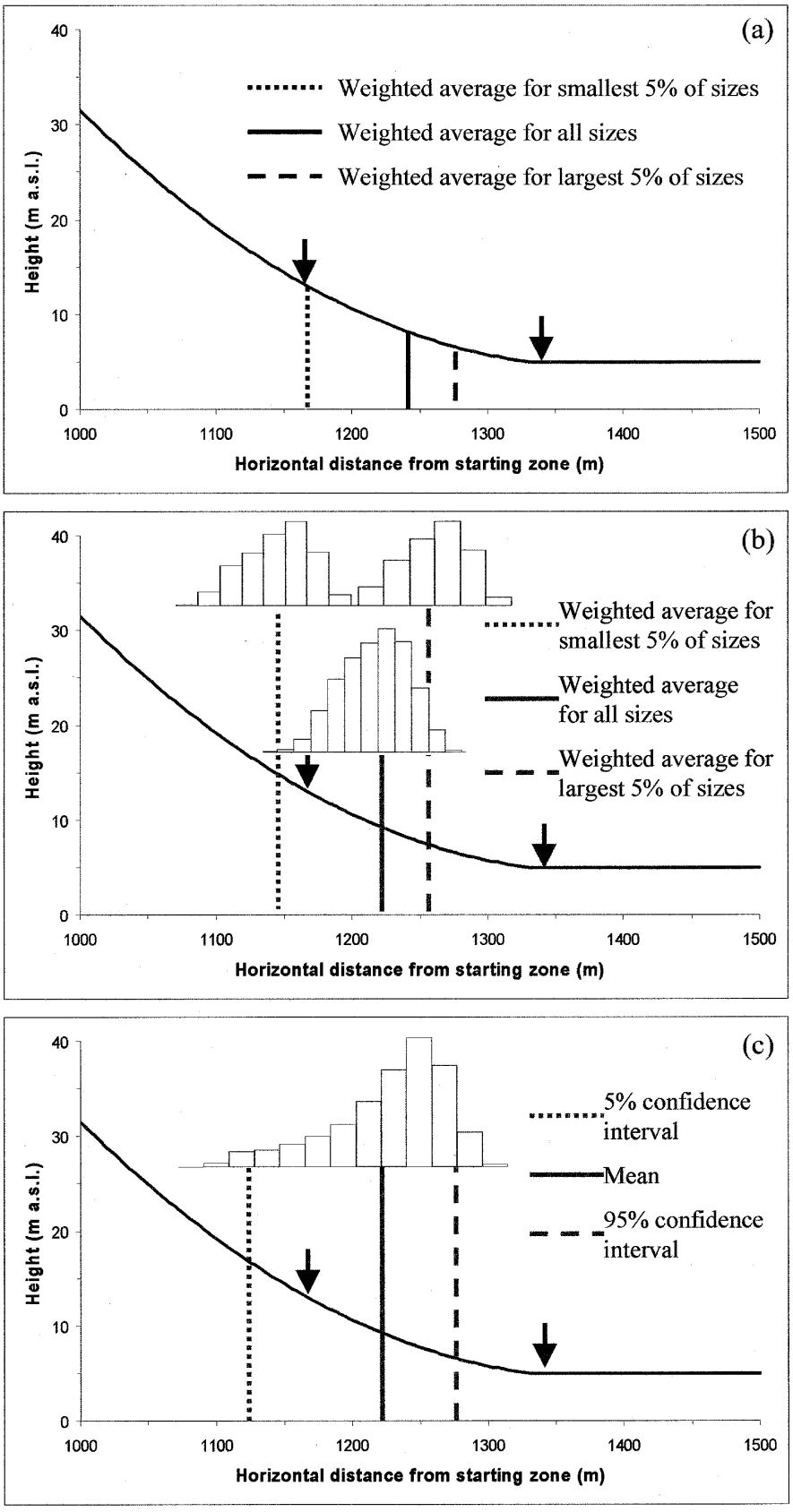

Fig. 6. The results from this study presented in three ways. See text for an explanation of each of these plots. The two arrows show the best-guess positions for $x(T = 30$ years) and $x(T = 300$ years).

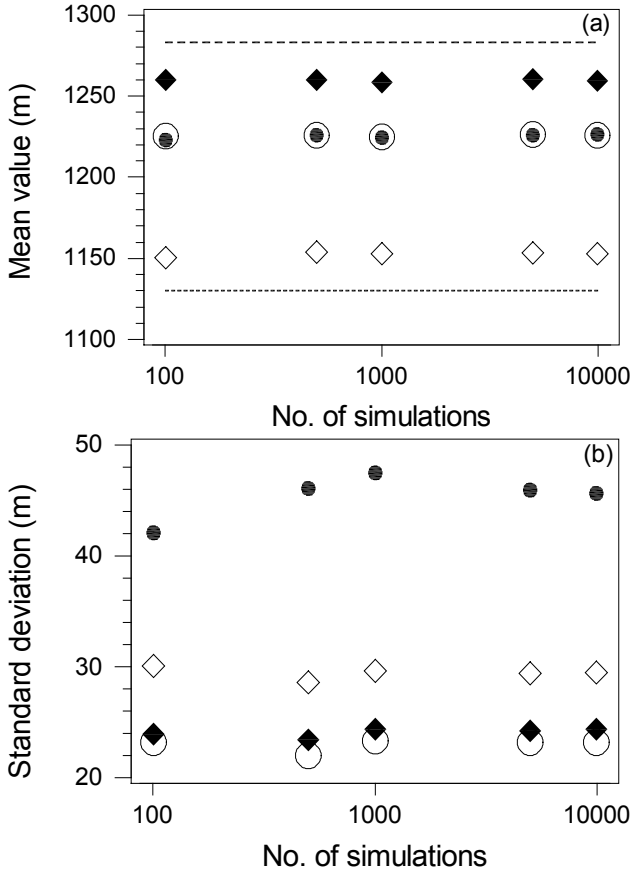

Fig. 7. Convergence of the study results with the number of simulations (on a logarithmic scale). The solid circles are for the full PDF (Fig. 6c), the open circles are the frequency-weighted average results of Fig. 6b, while the solid and open diamonds are the frequency-weighted average values for the upper and lower 5% distributions in Fig. 6b, respectively. The two lines on **(a)** indicate the position of the 90% confidence bands on the mean (dashed line: upper bond; dotted line: lower bond), taken from Fig. 6c for 10 000 simulations.

of Monte Carlo simulation, it can be seen that the frequency-weighted average value of $\overline{x}_{R/B}$ (Fig. 6b) appears to be quite close to the actual mean for $x_{R/B}(0.95)$ (Fig. 6c). There was no significant difference at the 5% significance level between the two mean values (assuming a Gaussian distribution) or between the two median values (with no distribution assumption). Conversely, the 90% confidence interval for $x_{R/B}$ (Fig. 6c) is approximately 50 m wider than that obtained by considering the frequency-weighted average value for $\overline{x}_{R/B}(0.05)$ and $\overline{x}_{R/B}(0.95)$ given in Fig. 6b. This is due to the difference between these two approaches: in Fig. 6c the full distribution is sampled, while Fig. 6b shows the variability in the weighted average values for the smallest and largest 5% of avalanches.

It is interesting to note that the value for $\overline{x}_{R/B}$ (1243 m) obtained using the best estimate for $x(T = 30$ years) and $x(T = 300$ years) (Fig. 6a) appears to be quite close to the median of the PDF of $x_{R/B}$ obtained by Monte Carlo Simulation, given in Fig. 6c (1237 m). This suggests that the best-guess estimate provides a useful indicator of the central tendency for $x_{R/B}$, even if the value for F is not well known. The lack of sensitivity of the median to the assumed distribution for F is shown in Table 1, where the properties of the PDF given in Fig. 6c are compared to a PDF where the estimates for $x(T = 30$ years) and $x(T = 300$ years) are believed to occur between $x(T = 3$ years) and $x(T = 300$ years), and $x(T = 30$ years) and x(T=3000 years), respectively. Note that some of the statistical properties of the PDF of $x_{R/B}$ listed in Table 1 (e.g. mean, median, standard deviation), as well as the value previously indicated for the best-guess estimate of $x(T = 30$ years) and $x(T = 300$ years), are given to an accuracy (of the order of the meter) that is actually unreasonable. This is done for the purposes of analysis only and does not imply that these variables can be calculated with such accuracy.

Table 1. Properties of the PDF of $x_{R/B}$ given in Fig. 6c (PDF_1) compared to a PDF where the estimates for $x(T = 30$ years) and $x(T = 300$ years) are believed to occur between $x(T = 3$ years) and $x(T = 300$ years), and $x(T = 30$ years) and $x(T = 3000$ years), respectively (PDF_2)

	PDF_1	PDF_2
Mean (m)	1226	1224
Median (m)	1237	1237
Standard deviation (m)	46	82
Skewness	−0.92	−0.79
Kurtosis	0.28	0.64
5% confidence bound (m)	1130	1064
95% confidence bound (m)	1283	1334

The precise results obtained using Monte-Carlo simulation can be dependent upon the number of simulations used. Figure 7a shows that the mean values used in this study converge rapidly (by $n \approx 1000$), while the standard deviation (Fig. 7b) requires a longer simulation time ($n \approx 5000$). In particular, this is true for the case illustrated in Fig. 6c, where three distribution functions are sampled from randomly (i.e. those used to locate $x(T = 30$ years) and $x(T = 300$ years), and to define the distribution of avalanche sizes at each random estimate for $x(T = 300$ years)), instead of two, as in the case of Fig. 6b (i.e. those used to locate $x(T = 30$ years) and $x(T = 300$ years)).

4 Conclusions

Figure 8 shows a map of Súdavik with the largest known historic avalanche events, the results of an alpha-beta model analysis (Lied and Bakkehi, 1980) using the relation derived by Jóhannessson (1998), and the results of a risk analysis performed by the Icelandic Meteorological Office (Jónasson et al., 1999), as well as the results from this study, taken from Fig. 6c. The best-guess estimate for $x(T = 300$ years) is

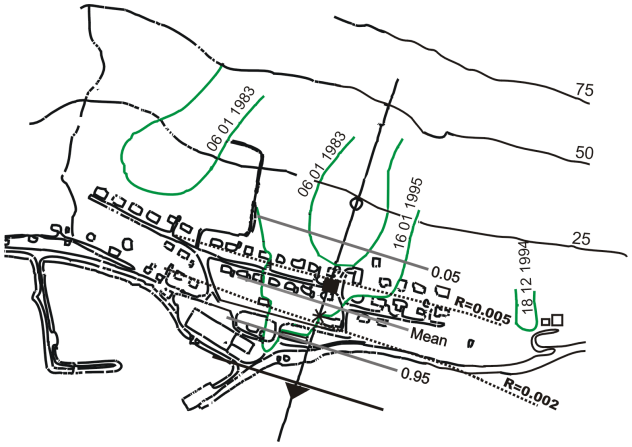

Fig. 8. A map of the Súdavik avalanche path showing the largest historical avalanches, the results of an alpha-beta model and of a risk analysis, and the positions for $x_{R/B}$ obtained in this study from Fig. 6c. The three grey lines are described in the text. The asterisk indicates the location of the median of $x_{R/B}$. The black solid line is the best-guess estimate for $x(T = 300$ years). The open circle is the predicted alpha point, and the solid square and solid triangle are alpha minus one standard deviation and alpha minus two standard deviations, respectively. The alpha-beta model simulations and the risk analysis were performed at the Icelandic Meteorological Office and are provided for comparative purposes.

marked with a black solid line and occurs at a similar position to the $\alpha - 2$ standard deviations. The three grey lines indicate $x_{R/B}(0.05)$, $E(x_{R/B})$ and $x_{R/B}(0.95)$ and are labelled '0.05', 'Mean', and '0.95', respectively. Our value for $E(x_{R/B})$ lies close to $\alpha - 1$ standard deviation and the 90% confidence bands seem to correspond to 1 standard deviation of α. It would be interesting to determine if such relations are true in general, since this would open the possibility of a practical interpretation of the alpha-beta model results within the Swiss zoning scheme. However, the fact that the alpha-beta model seems to perform relatively poorly upon this path would suggest that this may not be the case.

The optimum location for the red/blue zone boundary should be conservatively located downslope of $E(x_{R/B})$, but within the 90% confidence intervals. Table 1 shows that the median is a robust estimator of central tendency and, due to the negatively skewed distribution that results when return periods are translated into runout distances, it will always lie between $E(x_{R/B})$ and $x_{R/B}(0.95)$. Thus, for this path, a location 1237 m downslope is perhaps the optimum location for the red/blue zone boundary from our analysis. This appears to be close to the 2×10^{-3} risk contour line shown in Fig. 8, which equates to a return period of about 150 years (Jónasson et al., 1999), a recurrence interval that is sensible for the location of the red/blue hazard zones boundary.

The results that we have presented are only from one avalanche path. In order to investigate the usefulness of the approach outlined in this paper, testing many more paths is required. However, it is to be expected that for paths where the avalanche runout is adequately described by the statistical model and where the runout zone is of a smooth, continuous, approximately parabolic shape, the general conclusions from this study should hold true. Therefore, it should be possible to place confidence limits on the location for $x_{R/B}$ using our method. In the future, it may be possible to extend this approach to two dimensions using a more sophisticated dynamics model and a more complex statistical approach (Keylock et al., 1999). However, as runout distance is more commonly known to have a higher accuracy than the width, uncertainties in the width data underlying the statistical model and the greater difficulty in validating the dynamics model might make this problematic at the present time.

Acknowledgements. This paper is a contribution to the EU research project CADZIE (Catastrophic Avalanches, Defence Structure and Zoning in Europe), founded by the European Union under the contract n. EVG1-CT-1999-0009. We are grateful to the Icelandic Meteorological Office for their avalanche map of the Súdavik path and to M. M. Magnússon of the IMO for his help with this research. C. Harbitz of the Norwegian Geotechnical Institute provided many helpful comments. M. Barbolini acknowledges the support of the University of Pavia to enable him to travel to England in order to complete this project.

References

Barbolini, M., Gruber, U., Keyloch, C., Naaim, M., and Savi, F.: Application and evaluation of statistical and hydraulic-continuum dense-snow avalanche models to five real European sites, Cold Regions Science and Technology, 31, 2, 133–149, 2000.

Bartelt, P., Salm, B., and Gruber, U.: Calculating dense-snow avalanche runout using a Voellmy-fluid model with active/passive longitudinal straining, J. of Glac., 45, 150, 242–254, 1999.

BFF/SLF, Richtlinien zur Berücksichtigung der Lawinengefahr bei raumwirksamen Tätigkeiten, Bundesamt für Forstwesen and Eidgen. Institut für Schnee- und Lawinenforschung, EDMZ, CH-3000 Bern, 1984.

Jóhannesson, T.: Icelandic avalanche runout models compared with topographical models used in other countries. In Proceedings of the Anniversary Conference for the 25 Years of Snow Avalanche Research at NGI, Voss, Norway, 12–16 May 1998, NGI Publications No. 203, 43–52, 1998.

Jónasson, K., Sigurdson, S., and Arnalds, P.: Estimation of avalanche risk, Rit Vedurstofu Islands, VI-R99001-UR01, Reykjavik, 1999.

Keylock, C. J., McClung, D. M., and Magnússon, M. M.: Avalanche risk mapping by simulation, J. of Glac., 45, 150, 303–314, 1999.

Keylock, C. J. and Barbolini, M.: Snow avalanche impact pressure/vulnerability relations for use in risk assessment, Can. Geot. J., 38, 2, 227–238, 2001.

Lied, K. and Bakkehi, S.: Empirical calculation of snow-avalanche run-out distance based on topographic parameters, J. of Glac., 26, 94, 165–177, 1980.

McClung, D. M. and Lied, K.: Statistical and geometrical definition of snow avalanche runout, Cold Regions Science and Technology, 13, 2, 107–119, 1987.

McClung, D. M. and Schaerer, P. A.: The avalanche handbook, Seattle, WA, The Mountaineers, 1993.

Natale, L., Nettuno, L., and Savi, F.: Numerical simulation of dense snow avalanche: an hydraulic approach, In Hamza, M. H., ed. Proceedings of 24th International Conference on Modelling and Simulations, MS'94, 2–4 May, Pittsburgh, Pennsylvania, Anaheim, International Association of Science and Technology Development (IASTED) ACTA PRESS, 233–236, 1994.

Salm, B., Burkard, A., and Gubler, H.: Berechnung von Fliesslawinen: eine Anleitung für Praktiker mit Beispielen, Eidg. Inst. Schnee- und Lawinenforsch. Mitt., 47, 41, 1990.